J Mol Model (2012) 18:3941–3949
DOI 10.1007/s00894-012-1388-1

ORIGINAL PAPER

Density functional investigation of hydrogen gas adsorption on Fe−doped pristine and Stone−Wales defected single−walled carbon nanotubes

Chanukorn Tabtimsai · Somchai Keawwangchai · Nadtanet Nunthaboot · Vithaya Ruangpornvisuti · Banchob Wanno

Received: 7 January 2012 / Accepted: 21 February 2012 / Published online: 21 March 2012

Abstract The adsorptions of hydrogen molecule of the Fe−doped pristine and Stone−Wales defected armchair (5,5) single−walled carbon nanotubes (SWCNTs) compared with the pristine SWCNT were investigated by using the density functional theory at the B3LYP/LanL2DZ level. The doping of Fe atom into SWCNTs occurring via an exothermic process was found. The adsorptions of hydrogen molecule on the Fe−doped structures of either perfect or SW defected SWCNTs are stronger than on their corresponding undoped structures. The structural and electronic properties of the pristine and SW defected SWCNTs, their Fe−doped structures and their hydrogen molecule adsorptions are reported.

Keywords Adsorption · Carbon nanotube · DFT · Fe−doped · Stone−Wales defect

Introduction

Since the discovery of multi wall carbon nanotubes (MWCNTs) in 1991 [1] and single wall carbon nanotubes (SWCNTs) in 1993 [2], they have attracted the attention of the researchers due to their extraordinary structural, mechanical and electrical properties and a variety of potential applications including the hydrogen storage [3].

C. Tabtimsai · S. Keawwangchai · N. Nunthaboot · B. Wanno (✉)
Supramolecular Chemistry Research Unit, Department of Chemistry, Faculty of Science, Mahasarakham University, Mahasarakham 44150, Thailand
e-mail: banchobw@gmail.com

V. Ruangpornvisuti
The Postgraduate Education and Research in Chemistry (PERCH) Program and Department of Chemistry, Faculty of Science, Chulalongkorn University, Bangkok 10330, Thailand

Hydrogen is the cleanest energy source and in the future the hydrogen energy system is expected to progressively replace the existing fossil fuels. The suitable material used for hydrogen storage should be high storage capacity, release of hydrogen at room temperature and moderate pressure. One of the possible methods of hydrogen storage is the adsorption of hydrogen on materials with a large specific surface area such as carbon nanotubes (CNTs). Since the first experimental reported by Dillon and co−workers, hydrogen is storaged in CNTs [4]. The hydrogen adsorptions on the surfaces of SWCNTs have attracted considerable experimental and theoretical interest [5–11]. In order to enhance hydrogen storage capacity, the transition metal−doped SWCNTs and defected structures are adopted and much progress is made. Many of the research works reported that the foreign atoms [12] can be doping on the side wall of SWCNTs [13–15] including to Fe atom [16, 17]. The physisorption of hydrogen on SWCNT is found at low temperature [7]. The physisorption energies per hydrogen molecule decrease when the surface of SWCNTs is fully covered [8]. Hydrogen adsorption is found to be dependent on the micropore volume as well as the pore−size, larger micropore volumes showing higher hydrogen adsorption capacity [10]. The hydrogen adsorption on Pd−doped SWCNTs has been investigated and reported [11]. The binding energy of hydrogen storage capacity can be further enhanced by using the Pd−doped SWCNTs. Hydrogen adsorption on Eu−doped SWCNTs has also been calculated. The results indicate that five H_2 per Eu atom can be adsorbed in the Eu−doped SWCNT systems [18]. The theoretical study of the sidewall reactivity based on SWCNT in reacting with C_2H_4, O_2, and O_3 species illustrates that the central C−C bond of carbon ad−dimer defects in SWCNT is chemically more reactive than that of perfect sites (PS)

[19]. The 5−7−7−5 Stone−Wales (SW) defects are more highly reactive than perfect tube walls confirmed for the reaction with methylene [20, 21].

In the present work, the adsorption abilities for hydrogen gas on Fe−doped pristine and Stone−Wales defected armchair (5,5) SWCNTs compared with their corresponding undoped structures have been investigated by using the density functional theory (DFT) method. Structural and electronic properties for clean structures of pristine and SW−defected SWCNTs, their Fe−doped and their hydrogen gas adsorption structures have been determined and reported.

Computational details

The structural properties of perfect sited SWCNT (PS−SWCNT), Stone−Wales defected 7−5−5−7 SWCNT (SW1−SWCNT), Stone−Wales defected 5−7−7−5 SWCNT (SW2−SWCNT), Fe−doped perfect sited SWCNT (Fe−PS−SWCNT), Fe−doped SW1 SWCNT (Fe−SW1−SWCNT), Fe−doped SW2 SWCNT (Fe−SW2−SWCNT) and their hydrogen adsorptions (H_2/PS−SWCNT, H_2/SW1−SWCNT, H_2/SW2−SWCNT, H_2/Fe−PS−SWCNT, H_2/Fe−SW1−SWCNT and H_2/Fe−SW2−SWCNT) have been optimized by using the DFT method. The calculations with hybrid density functional B3LYP have recommended the Becke's three−parameter exchange functional [22] with the Lee−Yang−Parr correlation functional [23], using the Los Alamos LanL2DZ split−valence basis set [24–26]. All calculations were performed using GAUSSIAN 03 program [27]. The electronic properties of the undoped and Fe−doped SWCNTs and their hydrogen adsorptions were analyzed. The electronic densities of states (DOSs) for the undoped and Fe−doped SWCNTs and their hydrogen adsorption were investigated and plotted by the GaussSum 2.1.4 program [28]. The partial charge transfer (PCT) [29] during hydrogen adsorption which is defined as a change of hydrogen charges during adsorption by using natural bond orbital (NBO) analysis implemented in GAUSSIAN 03 program.

The binding energy (ΔE_b) of the Fe−doped SWCNT in the fully optimized geometry is obtained from Eq. 1.

$$\Delta E_b = E[\mathrm{Fe-SWCNT}] - E[\mathrm{SWCNT}] - E[\mathrm{Fe}] \quad (1)$$

Where E[Fe−SWCNT] is the total energy of the Fe−doped on a perfect or defected SWCNT, E[SWCNT] is the total energy of the perfect or defected SWCNT, and E[Fe] is the total energy of the isolated Fe atom.

The adsorption energies (ΔE_{ads}) of hydrogen molecule on undoped and Fe−doped perfect and SW−defected SWCNTs in the fully optimized geometry are calculated from Eqs. 2 and 3, respectively.

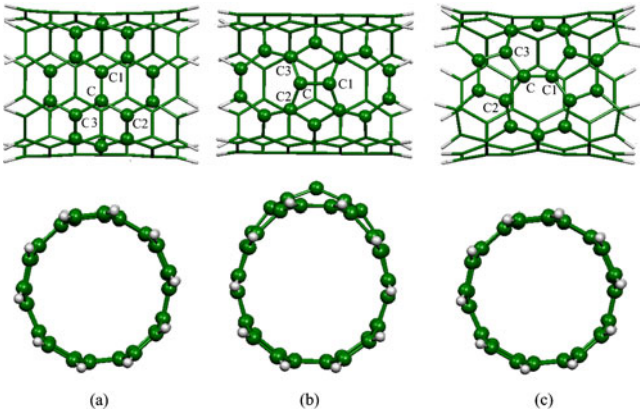

Fig. 1 The B3LYP/LanL2DZ optimized structures of (**a**) PS−SWCNT, (**b**) SW1−SWCNT and (**c**) SW2−SWCNT. Top and bottom are side and front views of tubes

$$\Delta E_{ads} = E[H_2/\mathrm{SWCNT}] - E[\mathrm{SWCNT}] - E[H_2] \quad (2)$$

$$\Delta E_{ads} = E[H_2/\mathrm{Fe-SWCNT}] - E[\mathrm{Fe-SWCNT}] - E[H_2] \quad (3)$$

Where E[H_2/SWCNT] is the total energy of the hydrogen adsorbed on a perfect or defected SWCNT, E[H_2/Fe−SWCNT] is the total energy of the hydrogen molecule adsorbed on a Fe doped perfect or defected SWCNT and E[H_2] is the total energy of the isolated hydrogen molecule.

Results and discussion

Geometries of the undoped and Fe−doped SWCNTs and their adsorptions with hydrogen molecule

The B3LYP/LanL2DZ optimized structures of undoped and Fe−doped SWCNTs are displayed in Figs. 1 and 2,

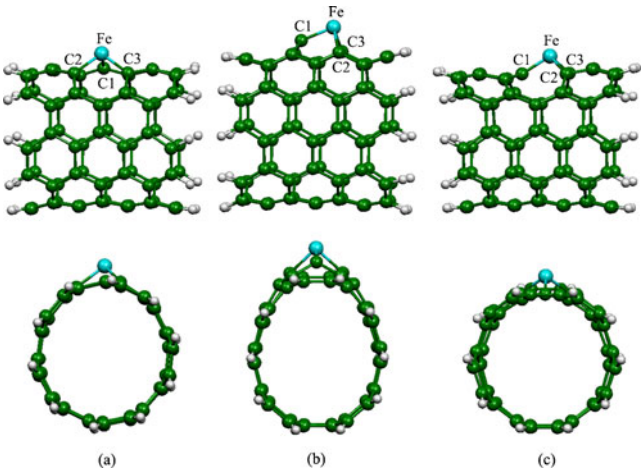

Fig. 2 The B3LYP/LanL2DZ optimized structures of the Fe−doped as (**a**) Fe−PS−SWCNT, (**b**) Fe−SW1−SWCNT and (**c**) Fe−SW2−SWCNT. Top and bottom are side and front views of tubes

Table 1 Selected geometrical parameters of the pristine and SW defected SWCNTs, their Fe−doped structures and their hydrogen adsorptions, computed at the B3LYP/LanL2DZ level

Species	Bond length (Å)			Binding distance (Å)	Bond angle (^{O})		
	C1−M[a,b]	C2−M[a,b]	C3−M[a,b]	M−H[b]	C1−M−C2	C2−M−C3	C3−M−C1
Species of PS−SWCNT:							
PS−SWCNT	1.418	1.442	1.441	−	118.6	120.3	118.6
Fe−PS−SWCNT	1.805	1.797	1.797	−	94.4	99.5	94.4
H_2/PS−SWCNT	1.418	1.441	1.441	3.142 (C−H1) 3.886 (C−H2)	118.7	120.2	118.7
H_2/Fe−PS−SWCNT	1.818	1.799	1.799	1.980 (Fe−H1) 2.016 (Fe−H2)	93.5	99.0	93.5
Species of SW1−SWCNT:							
SW1−SWCNT	1.406	1.468	1.468	−	108.9	120.7	108.9
Fe−SW1−SWCNT	1.782	1.884	1.884	−	85.2	91.6	85.2
H_2/SW1−SWCNT	1.406	1.468	1.468	3.442 (C−H1) 4.174 (C−H2)	108.9	120.7	108.9
H_2/Fe−SW1−SWCNT	1.786	1.888	1.888	2.096 (Fe−H1) 2.170 (Fe−H2)	84.5	88.8	84.5
Species of SW2−SWCNT:							
SW2−SWCNT	1.352	1.467	1.467	−	126.6	106.8	126.6
Fe−SW2−SWCNT	1.690	1.831	1.831	−	99.1	91.7	99.1
H_2/SW2−SWCNT	1.353	1.467	1.467	3.406 (C−H1) 4.168 (C−H2)	126.6	106.8	126.6
H_2/Fe−SW2−SWCNT	1.686	1.840	1.840	2.094 (Fe−H1) 2.094 (Fe−H2)	98.2	90.4	98.2

[a] C1, C2 and C3 are atoms on the SWCNTs which are defined in Fig. 1

[b] M is C atom for without Fe doping species and Fe metal which is doped on SWCNT species labeled in Figs. 1 and 2, respectively

respectively, and the selected geometrical parameters of the data of all optimized structures are tabulated in Table 1. The C1−Fe (1.805 Å), C2−Fe (1.797 Å) and C3−Fe (1.797 Å) bond lengths of Fe−doped SWCNTs are longer than C1−C (1.418 Å), C2−C (1.442 Å) and C3−C (1.441 Å) bond lengths of undoped SWCNTs. The C1−Fe−C2 (94.4°), C2−Fe−C3 (99.5°) and C3−Fe−C1 (94.4°) bond angles for Fe−doped SWCNTs are smaller compared to C1−C−C2 (118.7°), C2−C−C3 (120.2°) and C3−C−C1 (118.7°) bond angles of the undoped SWCNTs. Clearly, doping of Fe atom causes the deformation of the six−membered rings in the doping site of the SWCNTs and the SWCNT surfaces are protruding

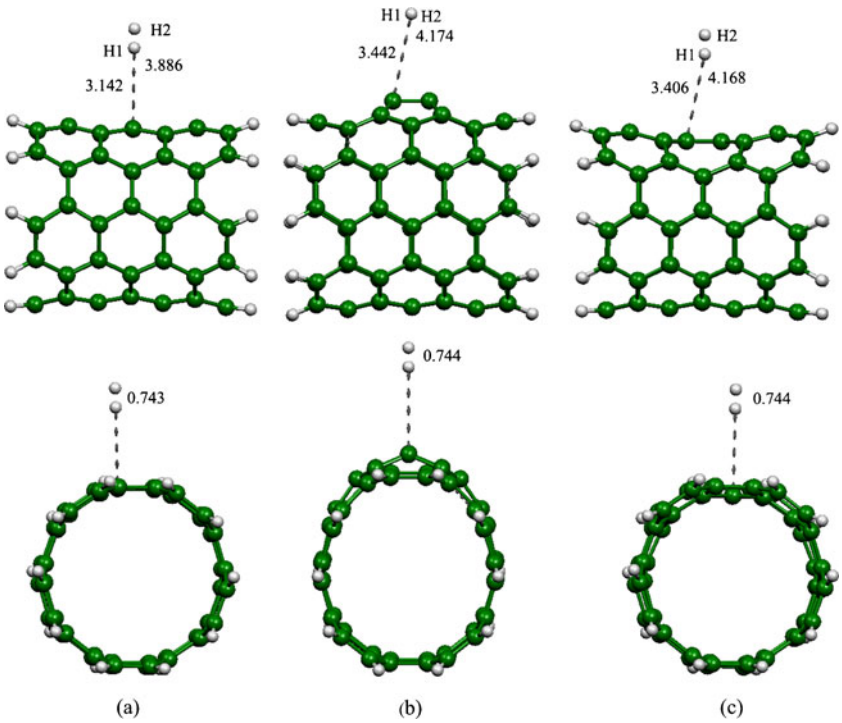

Fig. 3 The B3LYP/LanL2DZ optimized structures of the hydrogen molecule adsorption configurations of (**a**) H_2/PS−SWCNT, (**b**) H_2/SW1−SWCNT and (**c**) H_2/SW2−SWCNT. Top and bottom are side and front views of tubes. Bond distances are in Å

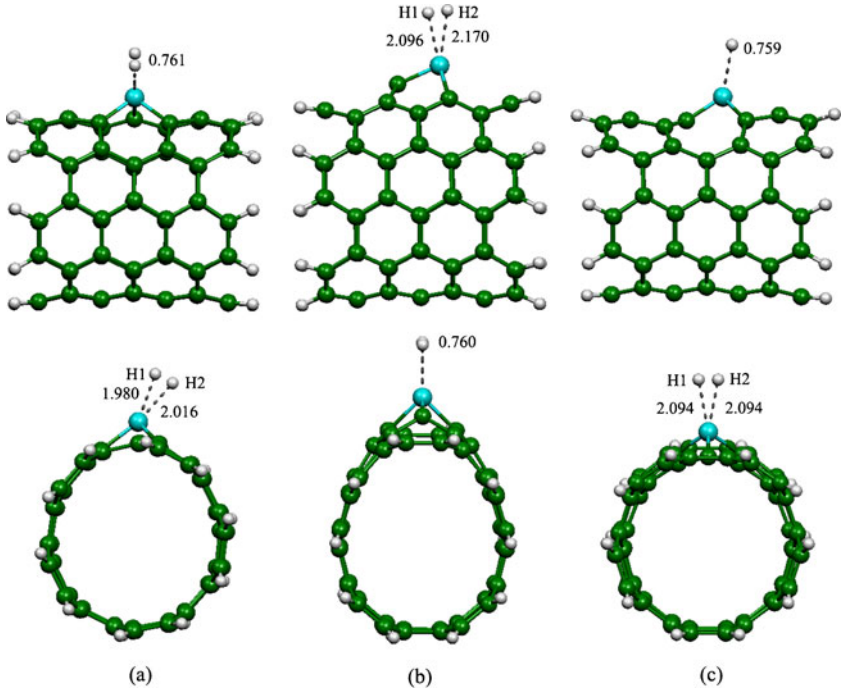

Fig. 4 The B3LYP/LanL2DZ optimized structures of the hydrogen molecule adsorption configurations of (**a**) H_2/Fe−PS−SWCNT, (**b**) H_2/Fe−SW1−SWCNT and (**c**) H_2/Fe−SW2−SWCNT. Top and bottom are side and front views of tubes. Bond distances are in Å

similarly to pyramidal structure. The buckling pattern of C−Fe sp^2 bonds in which C atoms slightly protrude Fe atom to out side surface is visible for all systems. The optimized structures of hydrogen molecule adsorbed on the undoped and Fe−doped SWCNTs computed at B3LYP/LanL2DZ level of theory are displayed in Figs. 3 and 4, respectively and the selected geometrical parameters are tabulated in Table 1. The adsorptions of hydrogen molecule on the undoped SWCNTs are not affected by the C1−C, C2−C and C3−C bond lengths. Whereas for the hydrogen molecule adsorbed on Fe−doped SWCNTs, the C1−Fe, C2−Fe and C3−Fe bond lengths are longer than that without hydrogen adsorptions. The adsorptions of hydrogen molecule on the undoped SWCNTs are not affected to C1−C−C2, C2−C−C3 and C3−C−C1 bond angles. Whereas the C1−Fe−C2, C2−Fe−C3 and C3−Fe−C1 bond angles of hydrogen molecule adsorbed on Fe−doped SWCNTs are narrowed compared to without hydrogen adsorptions. The results indicate that hydrogen adsorptions have more affect on the geometrical structures at the adsorption sites of Fe−doped SWCNTs than that of the undoped SWCNTs.

Table 2 Binding energies (ΔE_b) for Fe atom onto the pristine and SW defected SWCNTs, computed at the B3LYP/LanL2DZ level

Species	ΔE_b[a]
PS−SWCNT+Fe → Fe−PS−SWCNT	−188.99
SW1−SWCNT+Fe → Fe−SW1−SWCNT	−140.36
SW2−SWCNT+Fe → Fe−SW2−SWCNT	−219.36

[a] In kcal mol^{-1}

Binding energies of Fe−doped SWCNTs and adsorption energies of hydrogen molecule adsorbed on SWCNTs

The binding energies of Fe atom on the side wall SWCNTs are tabulated in Table 2. The binding energies of Fe−doped on perfect and defected SWCNTs indicate that the binding occurs via the exothermic processes. The binding strengths for Fe−doped PS−, SW1− and SW2−SWCNTs are in decreasing order: Fe−SW2−SWCNT (ΔE_b=−219.36 kcal mol^{-1})>Fe−PS−SWCNT (ΔE_b=−188.99 kcal mol^{-1})>Fe−SW1−SWCNT (ΔE_b=−140.36 kcal mol^{-1}). The SW2−SWCNT shows the highest reactive to Fe atom. The binding energy of Fe−doped SWCNTs in this study agrees well with the previous works [6, 30].

The adsorptions of hydrogen molecule on undoped and Fe−doped PS−, SW1− and SW2−SWCNTs occur via exothermic

Table 3 Adsorption energies (ΔE_{ads}) of hydrogen molecule onto the pristine and SW defected SWCNTs, their Fe−doped and their PCT, computed at the B3LYP/LanL2DZ level

Species	ΔE_{ads}[a]	PCT[b]
H_2/PS−SWCNT	−0.15	0.00
H_2/SW1−SWCNT	−0.17	0.00
H_2/SW2−SWCNT	0.02	0.00
H_2/Fe−PS−SWCNT	−5.49	0.08
H_2/Fe−SW1−SWCNT	−3.25	0.03
H_2/Fe−SW2−SWCNT	−3.88	0.05

[a] In kcal mol^{-1}

[b] Defined as a change of adsorbate's charges of H1+H2 during adsorption, in e

processes which are in good agreement with the previous works [12, 13, 15, 18, 31, 32], except for Fe−SW2−SWCNT species the adsorption occurs via an endothermic process indicating that the hydrogen molecule can not absorb on Fe−SW2−SWCNT. The adsorption energies and partial change transfers are tabulated in Table 3. The adsorption energies of hydrogen molecule on Fe−SWCNTs are higher than their corresponding undoped SWCNT clearly indicating that the doping of Fe atom improved the adsorption abilities of hydrogen on SWCNTs. The adsorption strengths are in the ranking of H_2/Fe−PS−SWCNT (ΔE_{ads}=−5.49 kcal mol^{-1})>H_2/Fe−SW2−SWCNT (ΔE_{ads}=−3.88 kcal mol^{-1}) ≈ H_2/Fe−SW1−SWCNT (ΔE_{ads}=−3.25 kcal mol^{-1})>H_2/SW1−SWCNT (ΔE_{ads}=−0.17 kcal mol^{-1}) ≈ H_2/PS−SWCNT (ΔE_{ads}=−0.15 kcal mol^{-1}) indicating that the Fe−PS−SWCNT species showed the highest suitable for hydrogen adsorptions. Moreover, the Fe−SW2−SWCNT is more reactive than Fe−SW1−SWCNT. For the undoped SWCNT system, the SW1−SWCNT is more reactive to hydrogen atoms than PS−and SW2−SWCNTs, respectively. It is shown that the sidewall reactivity of Fe−doped SWCNT toward the addition reaction increases with the increasing of pyramidalization angles, an indicator of deviation from sp^2 to sp^3 hybridization. The interaction between hydrogen and Fe−doped SWCNT is balanced by the electronic hybridization [18]. Thus, increasing of bond length (C−Fe) and pyramidalization angle at the doping site of the Fe−doped SWCNTs is expected to be more−reactive to hydrogen than the undoped SWCNTs, corresponding to the previous reports, in which Pd−[15] and Eu−doped [18] SWCNTs increase the hydrogen adsorption abilities of SWCNTs. The previous works, the adsorption energy of hydrogen molecule on Pd−doped SWCNT of −6.73 kcal mol^{-1} [15] and on Eu−doped SWCNT of values within the range of −6.00 to −11.30 kcal mol^{-1} [18] were found.

Electronic properties and partial charge transfer

The energies of the highest occupied molecular orbital (HOMO) E_{HOMO}, the lowest unoccupied molecular orbital (LUMO) E_{LUMO}, the frontier molecular orbital energy gaps (ΔE_{H-L}), global hardness (η), chemical potential (μ) and electrophilicity (ω) for the undoped and Fe−doped SWCNTs and their hydrogen adsorptions are tabulated in Table 4. Table 4 shows that the relative reactivity of hydrogen adsorbed on Fe−doped SWCNTs is in the order: H_2/Fe−SW1−SWCNT>H_2/Fe−SW2−SWCNT>H_2/Fe−PS−SWCNT, whereas the relative reactivity of hydrogen adsorbed on undoped SWCNT is in the order: H_2/PS−SWCNT=H_2/SW1−SWCNT>H_2/SW2−SWCNT. The ΔE_{H-L} of Fe−doped SWCNTs are lower than their corresponding undoped SWCNTs, indicating that the SWCNT clearly changes nearly to a conductor due to the doping of Fe atom. The energy gap of the hydrogen molecule adsorbed on PS−SWCNT, Fe−PS−SWCNT and Fe−SW2−SWCNT are larger than without hydrogen adsorption which is responsible for the weakened conductance. Plots of HOMOs and LUMOs of the Fe−doped PS−, SW1− and SW2−SWCNTs and their hydrogen adsorptions are displayed in Figs. 5 and 6, respectively. The plots show that the HOMOs of Fe−PS−SWCNT and their hydrogen adsorption are delocalized around the tube. Interestingly, the LUMOs of Fe−PS−SWCNT and their hydrogen adsorption are located over doping or adsorption sites. The electronic chemical potential is a measure of the tendency of electrons to escape a system and can be related to the energies of the HOMOs and LUMOs via Koopman's theorem [33], where I is the ionization potential and A is the electron affinity [34–36]. Due to the average local ionization energy ($\bar{I}$) was introduced as a means for identifying reactive sites on surface including carbon nanotubes, $\bar{I}$ has been connected to electronegativity, local polarizability and hardness. These characteristics are

Table 4 Chemical indices of the pristine and SW defected SWCNTs, their Fe−doped structures and their hydrogen adsorptions, computed at the B3LYP/LanL2DZ level

Species	E_{LUMO}[a]	E_{HOMO}[a]	ΔE_{H-L}[a]	$\Delta\Delta E_{H-L}$[a,b]	η[c]	μ[d]	ω[e]
Species of PS−SWCNT:							
PS−SWCNT	−2.748	−4.762	2.014	–	1.007	3.755	7.099
Fe−PS−SWCNT	−3.076	−4.872	1.605	–	0.802	3.879	6.036
H_2/PS−SWCNT	−2.667	−4.871	2.204	−0.19	1.102	3.769	7.827
H_2/Fe−PS−SWCNT	−2.884	−4.653	1.769	−0.16	0.884	3.769	6.281
Species of SW1−SWCNT:							
SW1−SWCNT	−2.939	−5.143	2.204	–	1.102	4.041	8.998
Fe−SW1−SWCNT	−2.939	−4.953	2.014	–	1.007	3.946	7.838
H_2/SW1−SWCNT	−2.939	−5.143	2.204	0.00	1.102	4.041	8.998
H_2/Fe−SW1−SWCNT	−2.884	−4.898	2.014	0.00	1.007	3.891	7.623
Species of SW2−SWCNT:							
SW2−SWCNT	−2.830	−4.898	2.068	–	1.034	3.864	7.720
Fe−SW2−SWCNT	−3.075	−4.735	1.660	–	0.830	3.905	6.328
H_2/SW2−SWCNT	−2.830	−4.898	2.068	0.00	1.034	3.864	7.720
H_2/Fe−SW2−SWCNT	−2.884	−4.708	1.823	−0.16	0.912	3.796	6.568

[a] In eV

[b] Defined as ΔE_{H-L}(H_2/SWCNT) − ΔE_{H-L}(SWCNT) and ΔE_{H-L}(H_2/Fe−SWCNT) − ΔE_{H-L}(Fe−SWCNT) for systems of SWCNT and Fe−doped SWCNTs, respectively

[c] η = Global hardness=(I−A)/2; I=−E_{HOMO} and A=−E_{LUMO}, respectively

[d] μ = Chemical potential=(I+A)/2

[e] ω = Electrophilicity = $\mu^2/2\eta$

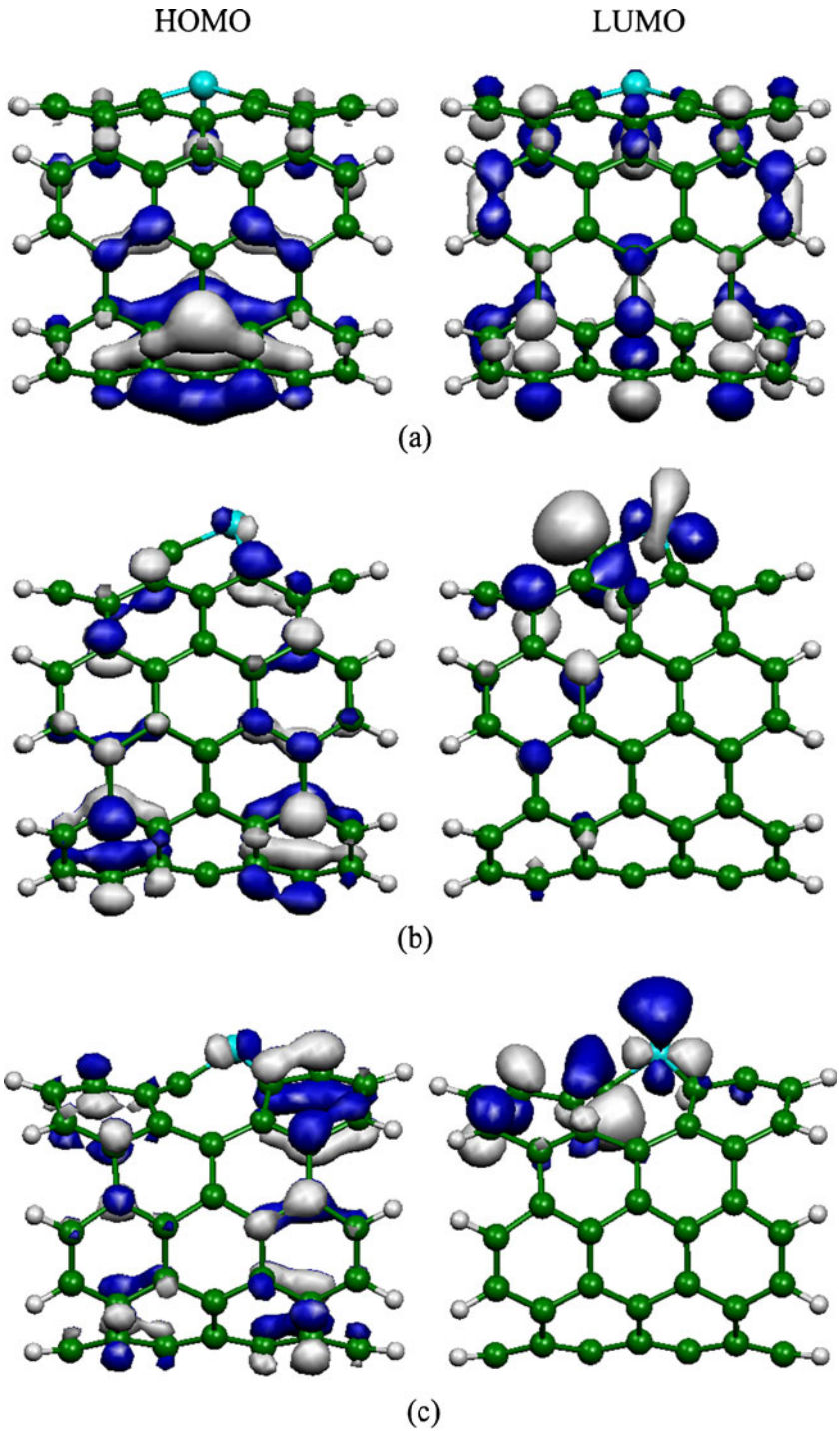

Fig. 5 The plots of HOMOs (left) and LUMOs (right) of (**a**) Fe−PS−SWCNT, (**b**) Fe−SW1−SWCNT and (**c**) Fe−SW2−SWCNT, computed at the B3LYP/LanL2DZ level

discussed in detail elsewhere [37]. The μ is also equal to the negative of Mulliken's electronegativity: the average of I and A [38]. The global hardness, chemical potential and electrophilicity for Fe−doped SWCNTs are in order: Fe−SW2−SWCNT> Fe−PS−SWCNT indicating that the Fe−PS−SWCNT is suitable for hydrogen adsorption.

The electronic densities of states for the undoped and Fe−doped SWCNTs with and without hydrogen adsorptions are plotted in Fig. 7 for better understanding the effect of creating defect, Fe doping and hydrogen adsorption to the electronic structure of SWCNTs. The electronic structures observed near Fermi level of the undoped SWCNTs (Figs. 7a–c), also show significant change due to the interaction with Fe atom (see Figs. 7d–f). The band gaps near Fermi level become sharply narrower and the peaks of the DOSs are nearly continuous, suggesting that the DOSs of undoped SWCNTs change nearly to a conductor due to the doping of Fe atom. It is clear that the presence of Fe atom decreases the energy gaps of the undoped

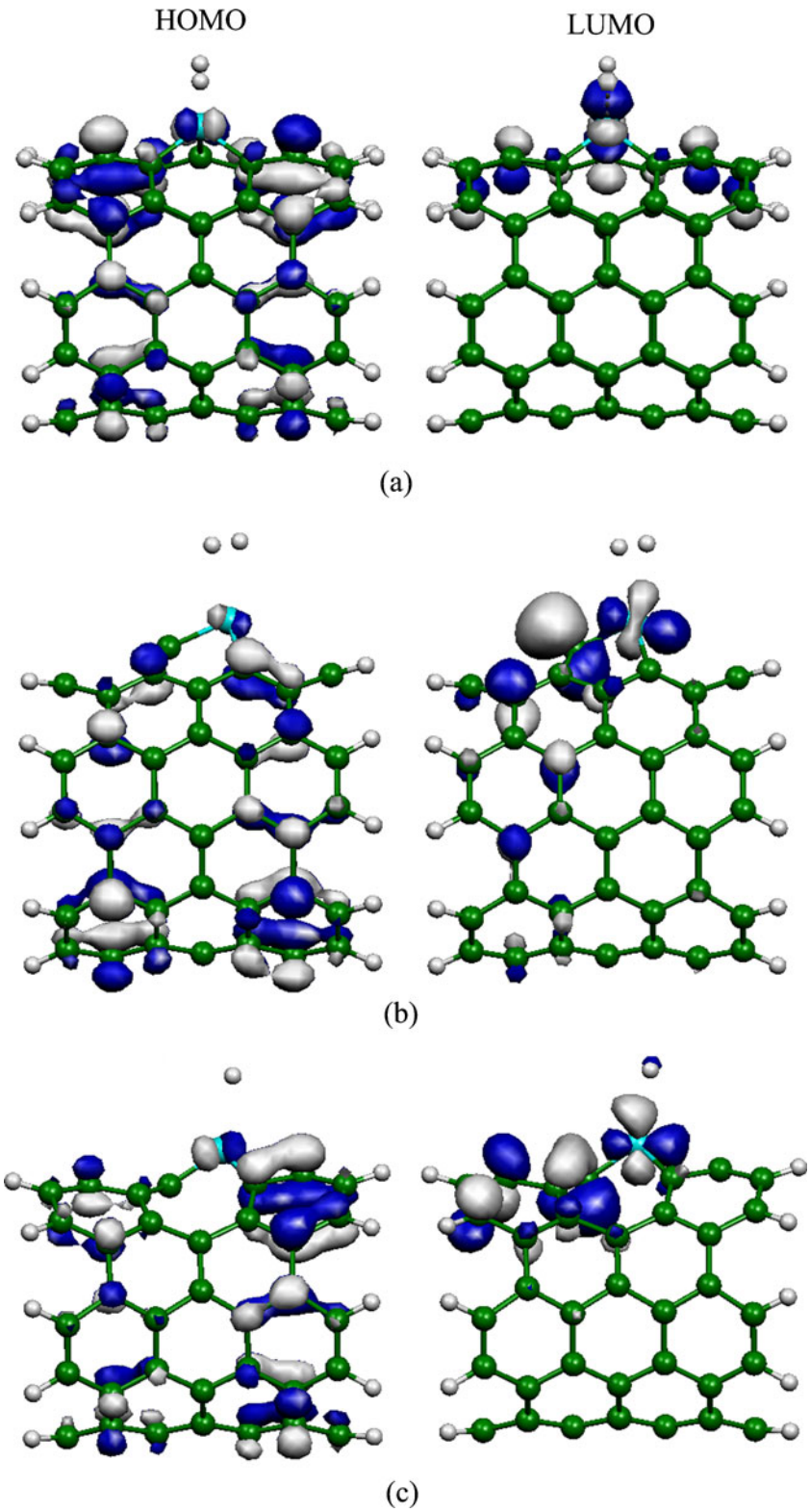

Fig. 6 The plots of HOMOs (left) and LUMOs (right) of hydrogen molecule adsorption configurations of (**a**) H_2/Fe−PS−SWCNT, (**b**) H_2/Fe−SW1−SWCNT and (**c**) H_2/Fe−SW2−SWCNT, computed at the B3LYP/LanL2DZ level

SWCNTs. The total DOSs of hydrogen molecule adsorbed on the undoped and Fe−doped SWCNT surfaces are displayed in Figs. 7g–l. The DOSs at around the Fermi level of hydrogen molecule adsorbed on undoped and Fe−doped SWCNTs are slightly changed compared to without hydrogen adsorptions.

In order to appreciate the interaction between Fe atom and SWCNTs as well as the interaction between hydrogen molecule and SWCNTs, it is instructive to analyze the partial charge transfer. The PCT is defined as the charge difference between the hydrogen molecule adsorbed on the SWCNTs and two

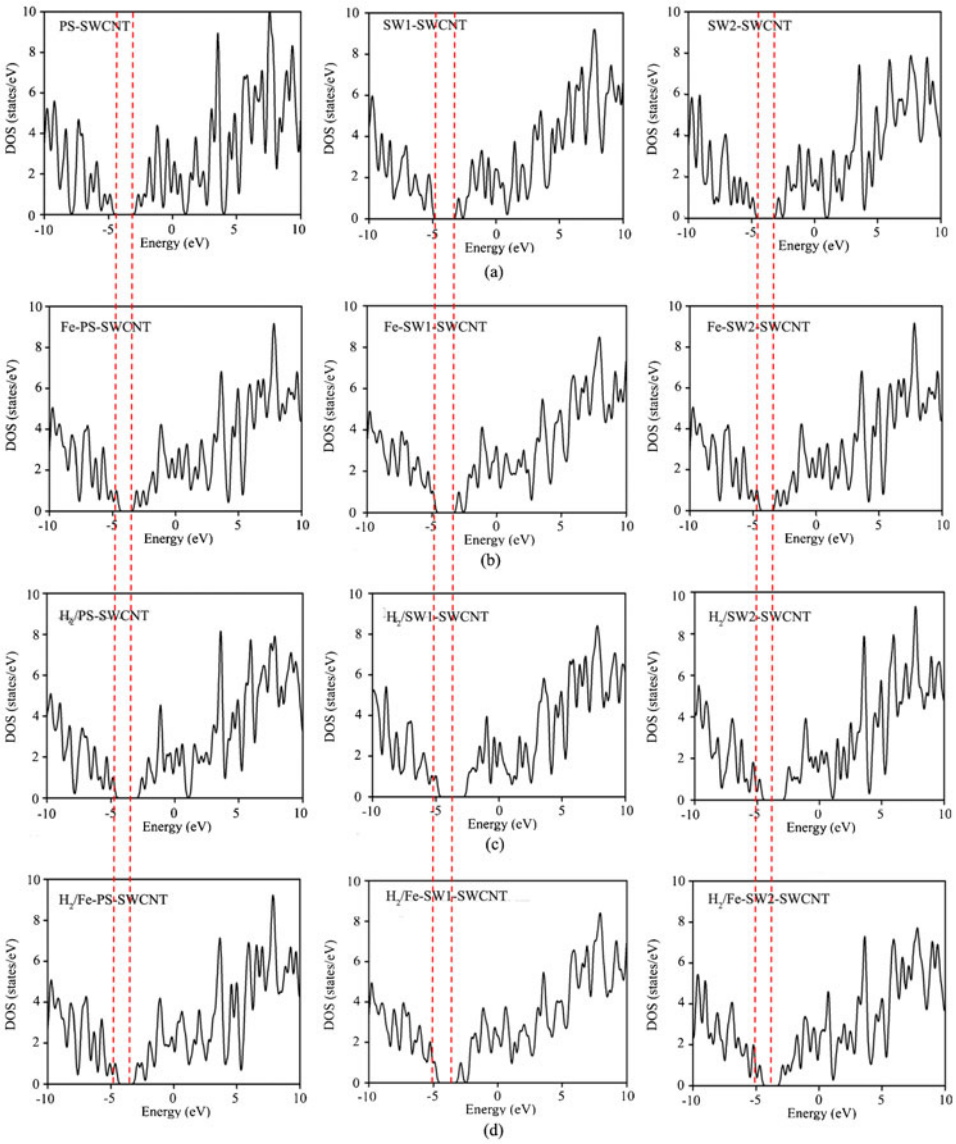

Fig. 7 The density of states of (**a**) PS−SWCNT, (**b**) SW1−SWCNT, (**c**) SW2−SWCNT, (**d**) Fe−PS−SWCNT, (**e**) Fe−SW1−SWCNT, (**f**) Fe−SW2−SWCNT, (**g**) H_2/PS−SWCNT, (**h**) H_2/SW1−SWCNT, (**i**) H_2/SW2−SWCNT, (**j**) H_2/Fe−PS−SWCNT, (**k**) H_2/Fe−SW1−SWCNT and (**l**) H_2/Fe−SW2− SWCNT

hydrogen atoms (see Table 3). The selected NBO charges for adsorption of hydrogen on Fe−doped SWCNT are tabulated in Table 5. Partial charge analysis indicates that most of the carbon atoms at the doping sites are the negative charges and most of

Table 5 Selected NBO charges (in *e*) of the adsorption structures of hydrogen molecule on the pristine and SW defected SWCNTs, their Fe−doped structures, computed at the B3LYP/LanL2DZ level

Species	C1[a]	C2[a]	C3[a]	M[b]	H1[c]	H2[c]
H_2/PS−SWCNT	−0.005	−0.009	−0.009	−0.008	0.002	−0.002
H_2/Fe−SWCNT	−0.019	−0.012	−0.012	0.367	0.067	0.013
H_2/SW1−SWCNT	−0.008	−0.017	−0.017	−0.008	0.011	−0.012
H_2/Fe−SW1−SWCNT	0.082	−0.108	−0.108	0.461	0.009	0.022
H_2/SW2−SWCNT	−0.020	−0.020	0.012	0.011	0.002	−0.002
H_2/Fe−SW2−SWCNT	0.082	−0.045	−0.045	0.389	0.027	0.027

[a] C1, C2 and C3 are atoms on the SWCNT which are defined in Fig. 1

[b] M is C atom without Fe doping systems and Fe metal which is doped on SWCNT systems labeled in Figs. 1 and 2, respectively

[c] H1 and H2 are atoms adsorbed on SWCNT and Fe−doped SWCNT which are defined in Figs. 3 and 4

the hydrogen atoms are positive. The PCTs of hydrogen molecule to SWCNT in these six structures are very small, suggesting that the interaction between the hydrogen molecule and SWCNT is intrinsically electrostatic. The PCTs from hydrogen molecule to Fe−doped SWCNTs are clearly larger than that of the undoped SWCNTs, which again proves that the doping of the Fe atom largely influences the electronic transport properties of the undoped SWCNTs. For doping species, when the PCT increases, the adsorption energy is also increased indicating that the large charge transfers result in the high adsorption energy. The results of PCT of CO adsorbed Al−doped SWCNT agrees well with this work which reported that the charge−transfer from a CO molecule to Al−doped SWCNT is clearly larger than that of the undoped SWCNT [39].

Conclusions

The interactions of hydrogen molecule with perfect sited SWCNT (PS−SWCNT), Stone−Wales defected 7−5−5−7 SWCNT (SW1−SWCNT), Stone−Wales defected 5−7−7−5 SWCNT (SW2−SWCNT) [21] and their Fe doping were investigated by using the density functional theory at the B3LYP/LanL2DZ level. The doping of Fe atom in SWCNTs occurs via exothermic process. The hydrogen molecule adsorptions of the Fe−doped SWCNTs are stronger than on the undoped SWCNTs. The structural and electronic properties of the undoped and Fe−doped SWCNTs and their adsorptions of hydrogen molecule are reported. The present results will provide useful guidance to develop novel SWCNT−based on hydrogen storage.

Acknowledgments The authors gratefully acknowledge the Research Affairs, Mahasarakham University, and the Postgraduate Education and Research in Chemistry (PERCH) program, Thailand, for financial support of this research and the facility provided by Supramolecular Chemistry Research Unit and Department of Chemistry, Faculty of Science, Mahasarakham University. The Thailand Research Fund for financial support (Grant No. MRG5180141) to BW is also acknowledged.

References

1. Iijima S (1991) Nature 354:56–58
2. Iijima S, Ichihashi T (1993) Nature 363:603–605
3. Darkrim FL, Malbrunota P, Tartaglia GP (2002) Int J Hydrog Energy 27:193–202
4. Dillon AC, Jones KM, Bekkedahl TA, Kiang CH, Bethune DS, Heben MJ (1997) Nature 386:377–379
5. Zhou LG, Shia SQ (2003) Carbon 41:579–625
6. Zhuang HL, Zheng GP, Soh AK (2008) Comput Mater Sci 43:823–828
7. Wang G, Huang Y (2008) J Phys Chem C 112:9128–9132
8. Yang SH, Shin WH, Lee JW, Kim SY, Woo SI, Kang JK (2006) J Phys Chem B 110(28):13941–13946
9. Khare BN, Meyyappan M, Cassell AM, Nguyen CV, Han J (2002) Nano Lett 2:73–77
10. Zhang G, Qi P, Wang X, Lu Y, Mann D, Li X, Dai H (2006) J Am Chem Soc 128:6026–6027
11. Sudan P, Züttel A, Mauron P, Emmenegger C, Wenger P, Schlapbach L (2003) Carbon 41:2377–2383
12. Cabria I, López MJ, Alonso JA (2006) Comput Mater Sci 35:238–242
13. Han SS, Lee HM (2004) Carbon 42:2169–2177
14. Yang YX, Singh RK, Webley PA (2008) Adsorption 14:265–274
15. Xiao H, Li SH, Cao JX (2009) Chem Phys Lett 483:111–114
16. Liu B, Weia L, Dinga Q, Yao J (2005) J Cryst Growth 277:293–297
17. Zhao X, Kadoya T, Ikeda T, Suzuki T, Inoue S (2007) Diamond Relat Mater 16:1101–1105
18. Zhang ZW, Li JC, Jiang Q (2010) J Phys Chem C 114:7733–7737
19. Horner DA, Redfern PC, Sternberg M, Zapol P, Curtiss LA (2007) Chem Phys Lett 450:71–75
20. Bettinger HF (2005) J Phys Chem B 109:6922–6924
21. Dinadayalane TC, Murray JS, Concha MC, Politzer P, Leszczynski J (2010) J Chem Theor Comput 6:1351–1357
22. Becke AD (1993) J Chem Phys 98:5648–5652
23. Lee C, Yang W, Parr RG (1988) Phys Rev B 37:785–789
24. Hay PJ, Wadt WR (1985) J Chem Phys 82:270–283
25. Wadt WR, Hay PJ (1985) J Chem Phys 82:284–298
26. Hay PJ, Wadt WR (1985) J Chem Phys 82:299–310
27. Frisch MJ et al. (2008) Gaussian03, Revision E.01. Gaussian Inc, Pittsburgh
28. O'Boyle NM, Tenderholt AL, Langner KM (2008) J Comput Chem 9(5):839–845
29. Marichev VA (2009) Colloids Surf A Physicochem Eng Asp 348:28–34
30. Meng FY, Zhou LG, Shi S-Q, Yang R (2003) Carbon 41:2023–2025
31. Yildirim T, Ciraci S (2005) Phys Rev Lett 94:175501–175504
32. Gayathri V, Geetha R (2007) Adsorption 13:53–59
33. Koopmans T (1933) Physica 1:104–113
34. Pearson RG (1963) J Am Chem Soc 85:3533–3543
35. Parr RG, Pearson RG (1983) J Am Chem Soc 105:7512–7516
36. Pearson RG (2005) J Chem Sci 117:369–377
37. Politzer P, Murray JS, Bulat FA (2010) J Mol Model 16:1731–1742
38. Mulliken RS (1934) J Chem Phys 2:782–793
39. Wang R, Zhang D, Sun W, Han Z, Liu C (2007) J Mol Struc THEOCHEM 806:93–97